High-resolution x-ray guided three-dimensional diffuse optical tomography of joint tissues in hand osteoarthritis: Morphological and functional assessments

Zhen Yuan[a] and Qizhi Zhang
Department of Biomedical Engineering, University of Florida, Gainesville, Florida 32611

Eric S. Sobel
Division of Rheumatology, College of Medicine, University of Florida, Gainesville, Florida 32611

Huabei Jiang[b]
Department of Biomedical Engineering, University of Florida, Gainesville, Florida 32611

(Received 27 April 2010; revised 9 June 2010; accepted for publication 2 July 2010; published 28 July 2010)

Purpose: The aim of this study was to investigate the potential use of multimodality functional imaging techniques to identify the quantitative optical findings that can be used to distinguish between osteoarthritic and normal finger joints.
Methods: Between 2006 and 2009, the distal interphalangeal finger joints from 40 female subjects including 22 patients and 18 healthy controls were examined clinically and scanned by a hybrid imaging system. This system integrated x-ray tomosynthetic setup with a diffuse optical imaging system. Optical absorption and scattering images were recovered based on a regularization-based hybrid reconstruction algorithm. A receiver operating characteristic curve was used to calculate the statistical significance of specific optical features obtained from osteoarthritic and healthy joints groups.
Results: The three-dimensional optical and x-ray images captured made it possible to quantify optical properties and joint space width of finger joints. Based on the recovered optical absorption and scattering parameters, the authors observed statistically significant differences between healthy and osteoarthritis finger joints.
Conclusions: The statistical results revealed that sensitivity and specificity values up to 92% and 100%, respectively, can be achieved when optical properties of joint tissues were used as classifiers. This suggests that these optical imaging parameters are possible indicators for diagnosing osteoarthritis and monitoring its progression. © *2010 American Association of Physicists in Medicine*.
[DOI: 10.1118/1.3467755]

Key words: diffuse optical tomography, x-ray, multimodality imaging, finger joint, bone

I. INTRODUCTION

Osteoarthritis (OA) is the most common arthritic condition worldwide and is estimated to affect nearly 60×10^6 Americans.[1–3] Classically, OA is most often found in the large weight-bearing joints of the lower extremities, particularly the knees and hips. However, there is also a subset of individuals with a predilection for developing OA of the hand and a more generalized form of OA.[3] Interestingly, this subgroup of patients usually has demonstrable joint erosions, which are best appreciated in the small joints of the hand. Traditionally, erosive OA as seen in this group has been viewed as an inflammatory variant and has also been termed inflammatory OA.[4] It is generally a polyarthropathy that classically involves the distal and proximal interphalangeal finger joints.

To diagnose cartilage abnormalities and alterations in the composition of synovial fluid in finger joints affected by OA, a variety of imaging methods have been developed and tested, such as x ray (conventional radiography), ultrasound, computed tomography, and magnetic resonance imaging.[5–9] Of all the existing imaging modalities, conventional radiography (CR) is the traditional first line and mainstay technique for the radiologic investigation of patients with inflammatory arthritis.[10] CR is also currently the reference standard in imaging for the detection and quantification of joint destruction in patients with OA.[4] CR is widely accessible largely due to its high resolution (~0.1 mm), low cost, and ease of use for multiple-joint assessment. It also provides information rapidly that can be used for both baseline evaluation and long-term follow-up of patients. Most drug trials in inflammatory arthritis use it as the major determinant of structural damage, as recommended by professional and regulatory authorities. While CR has extremely high resolution in differentiating bones from soft tissues, it cannot distinguish well between soft tissues of similar densities, as the imaging contrast between different soft tissues is very low. For example, while plain radiographs are able to visualize joint space narrowing and osteophyte formation, they are insensitive to changes in cartilage and associated soft tissues and therefore incapable of capturing the primary features of each stage of OA. Additionally, although current therapy is symptomatic and one could argue that early detection would not alter clinical care,

remarkable advances have been made in our understanding of the pathophysiology of OA and offer promise for new therapeutic directions.[11,12] Early diagnosis of OA in finger joints can also be of clinical importance, as it may help avoid unnecessary or expensive examinations and risky or unhelpful therapies. As such, highly sensitive and specific imaging methods are urgently needed for the detection of early stage changes in OA. The new imaging approaches should have the ability to demonstrate a reduction of joint destruction earlier than CR, which will be of great importance in assessing new forms of treatment.

Due to its numerous advantages of low cost, portability, and nonionizing radiation,[13–19] near-infrared diffuse optical tomography (DOT) is emerging as a potential tool for imaging bones and joint tissues.[20–23] DOT is a model-based medical imaging modality which uses near-infrared light to generate quantitative optical images of tissues. This technique measures the absorption of light, which is related to concentration of hemoglobin and oxygen saturation, and the scattering of light, which is related to the cellular morphology. So the optical imaging methods are able to provide a variety of functional and structural information with high sensitivity and specificity compared to other imaging modalities. This is especially true for the joints of the fingers, where the small dimensions and much higher transmitted light intensities should result in better signal-to-noise ratio and greatly improved spatial resolution. In a recent pilot case study, we have shown that the optical contrast between OA and normal joints is high,[21] suggesting that DOT has indeed the potential for detecting OA joints in the hands and assessing its treatment. While DOT appears to be especially suited for the imaging of the finger joints because of the high signal-to-noise ratio associated with the small volume, the spatial resolution is relatively low due to light scattering. Thus it is now clear that DOT can provide high-contrast joint tissue imaging with low resolution, while CR can offer high-resolution joint structure with low contrast in soft tissues. To take advantage of the complementary information from these two imaging modalities, an optimized approach that combines CR and DOT imaging has been developed for a case study of OA in the finger joints.[23] The basic idea of this multimodality approach is to incorporate the high-resolution structural CR images into the DOT reconstruction so that both the resolution and quantitative accuracy of optical image reconstruction are enhanced.

In this present study, we will go beyond the previous case validations and perform a small pilot clinical study of OA. Our purpose was to employ CR-guided DOT to investigate the typical optical findings that can be used to distinguish between OA and healthy finger joints. The final goal of this investigation is to utilize this hybrid functional imaging technique for the noninvasive detection of early stage OA and monitoring the efficacy of its treatment.

II. MATERIALS AND METHODS

II.A. Study subjects

Forty subjects were enrolled in the study between 2006 and 2009: 22 patients with OA and 18 healthy volunteers. All subjects (female; mean age 51 yr; age range 32–80) signed informed consent forms before participating in the study. Subjects were contacted either directly at the rheumatology outpatient clinics or via leaflets and posters that were distributed in the clinics. The clinical study was approved by the Institutional Review Board of University of Florida.

II.B. Clinical examination

Clinical examination of each patient was performed by a single experienced rheumatologist (E.S.S) at The University of Florida. Patients with OA were identified by the clinical features of bony thickening of the distal interphalangeal (DIP) finger joint and the absence of other arthropathies, including rheumatoid arthritis, psoriatic arthritis, and gout, as well as any traumatic injury to the joint that was selected for imaging. The control group consisted of 18 healthy volunteers who had no known OA or other joint diseases. Only one DIP finger joint of each subject was optically scanned in this initial study.

II.C. CR-guided DOT imaging

II.C.1. CR and optical imaging data acquisition

The hybrid CR/DOT imaging system that has been described in detail previously[21,23] integrates a modified mini C-arm CR system (MiniView 6800, GE-OEC, Salt Lake City, UT) with a homemade 64×64-channel photodiodes-based CW DOT system [see Fig. 1(a)]. The tomosynthetic imaging is realized through the modified C-arm CR system. Tomographic CR images are reconstructed from 2D projections using an improved shift-and-add algorithm we developed previously.[24] In this algorithm, we first segment or normalize the projection images and then apply the shift-and-add algorithm on the segmented projection images at multiple angles, which results in accurate reconstruction of the three-dimensional (3D) structures of joints. The CW-based DOT system consists of laser modules, a hybrid light delivery subsystem, a fiber optics/tissue interface, a data acquisition module, and light detection modules.[21] While the system has eight diode lasers (B&W TEK Inc., Newark, DE and Power Technology Inc., Little Rock, AR) with wavelengths from 634 to 974 nm working as light sources, this investigation used the measurement at 853 nm with a maximum output of 210 mW. The light intensity was measured as 70 mW when it was delivered to the fiber optical interface, and further reduced to 10–30 mW at the surface of the finger, which depended on the location of the finger relative to an excitation source position. The cylindrical fiber optics/tissue interface is composed of 64 source and 64 detector fiber bundles that are positioned in four layers along the surface of a Plexiglass container and cover a volume of 15×30 mm^2. In each layer, 16 source and 16 detector fiber bundles are alternatively arranged. The space between the finger and the wall of the Plexiglass container is filled with tissuelike phantom materials as coupling media consisting of distilled water, agar powder, Indian ink, and Intralipid, giving an absorption coefficient of 0.014 mm^{-1} and a reduced scattering coefficient of 1.0 mm^{-1}.[23]

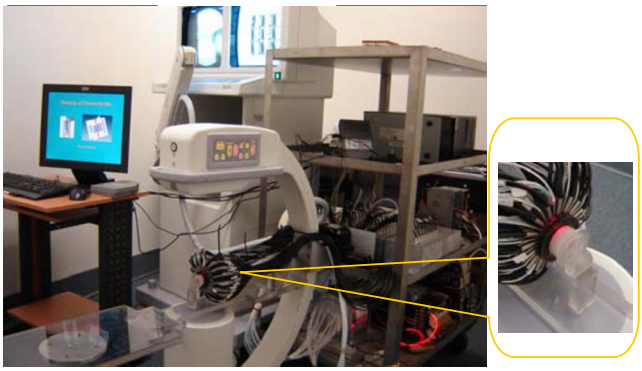

(a)

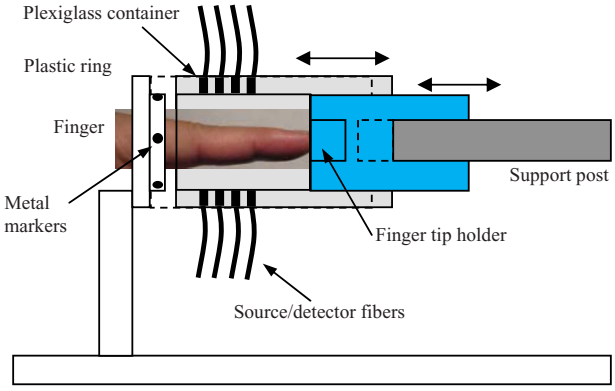

(b)

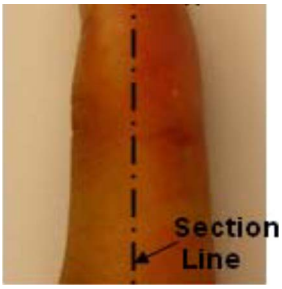

(c)

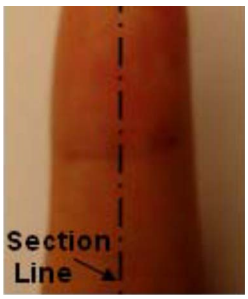

(d)

FIG. 1. (a) Photograph of the integrated hybrid x-ray/DOT system. The inset (right part) is a close-view photograph of the finger/fiber optics/x-ray interface. (b) Schematic of the interface. Note that both the Plexiglass container and finger tip holder can be translated horizontally for separate DOT and x-ray data acquisition. (c) The sagittal plane of a 3D DIP finger joint. (d) The coronal plane of a 3D DIP finger joint.

In the hybrid imaging of joint tissues, the CR imaging is performed immediately after the DOT data acquisition. To eliminate the artifacts in the CR projections possibly caused by the optical interface, we have used a coaxial post to support the optical interface, such that the interface can be translated along the post [see the inset in Fig. 1(a) and the schematic of the interface shown in Fig. 1(b)]. During an exam, the subject first places the finger into the Plexiglass container through a plastic ring while the distal end of the finger rests against a finger tip holder installed at the end of the coaxial post. Then, the optical interface is slid forth to be in contact with the plastic ring structure that is used to lock the position of the optical interface. Immediately after the DOT imaging, the optical interface is slid back for CR exposure while the finger stays at the same position. Four small metal spheres (1 mm in diameter) are embedded along the surface of the plastic ring as fiducial markers for accurate coregistration of the CR and optical imaging.

II.C.2. Image reconstruction algorithm

When the imaging data acquisition was finished, the next step was to generate the CR-guided optical images based on a robust 3D reconstruction algorithm.[23] We have developed a hybrid regularization-based scheme for CR-guided DOT image reconstruction, which is able to handle the cases where CR is insensitive to the target tissues or lesions.[23] For example, in the area of joint imaging, CR is not able to detect

the cartilage and fluids as well as other soft tissue changes surrounding joint cavity, although the changes associated with the soft tissues can be easily captured by DOT alone.

Our existing reconstruction algorithm is based on the following diffusion equation and type-III BCs:

$$\nabla \cdot D(r)\nabla\Phi(r) - \mu_a(r)\Phi(r) = -S(r), \tag{1}$$

$$-D\nabla\Phi\cdot n = \alpha\Phi, \tag{2}$$

where $\Phi(r)$ is the photon density, $D(r)$ the diffusion coefficient, α is a coefficient related to the internal reflection at the boundary, $\mu_a(r)$ is the absorption coefficient, and $S(r)$ is the source term. For the point source model, $S=S_0\delta(r-r_0)$ is used, where S_0 is the source strength and $\delta(r-r_0)$ is the Dirac delta function for a source at r_0. The diffusion coefficient can be written as $D=1/(3(\mu_a+\mu_s'))$, where μ_s' is the reduced scattering coefficient.

For CR-guided DOT reconstruction, the following updating equation is used for the inverse problem:[23]

$$\Delta\boldsymbol{\chi} = (\mathbf{J}^T\mathbf{J} + \mathbf{J}^T\mathbf{J} + \lambda' I + \mathbf{L}^T\mathbf{L})^{-1}[\mathbf{J}^T(\boldsymbol{\Phi}^o - \boldsymbol{\Phi}^c)], \tag{3}$$

where $\mathbf{J}$ is the Jacobian matrix formed by $\partial\Phi/\partial\chi$ at the boundary measurement sites. λ' is a scalar and I is the identity matrix. $\Delta\boldsymbol{\chi}=(\Delta D_1,\Delta D_2,\ldots,\Delta D_n,\Delta\mu_{a,1},\Delta\mu_{a,2},\ldots,\Delta\mu_{a,N})^T$ and $\Delta\boldsymbol{\chi}$ is the updating vector for the optical properties. $\boldsymbol{\Phi}^o=(\Phi_1^o,\Phi_2^o,\ldots,\Phi_M^o)^T$ and $\boldsymbol{\Phi}^c=(\Phi_1^c,\Phi_2^c,\ldots,\Phi_M^c)^T$, where $\boldsymbol{\Phi}_i^o$ and $\boldsymbol{\Phi}_i^c$, are observed and computed photon density for $i=1,2\ldots,M$ boundary locations. The x-ray *a priori* spatial information is incorporated into the iterative process using the spatially variant filter matrix $\mathbf{L}$. In this study, the Laplacian-type filter matrix was used and its elements L_{ij} were constructed according to the visible region or tissue type it was associated with CR derived priors as follows:

$$L_{ij} = \begin{cases} 1 & \text{when } i=j \\ -1/nn & \text{when } i,j\subset \text{one region} \\ 0 & \text{when } i,j\subset \text{different region} \end{cases}, \tag{4}$$

where nn is the finite element node number within a tissue type.

II.C.3. Image analysis methods

Image reconstruction of the DIP finger joint with the optical coupling phantom/media ($\pi 15^2\times 20$ mm^3 in volume) was performed with a finite element mesh of 2705 nodes and 13 440 tetrahedral elements for each of the 40 subjects. The 3D CR images of the joint allowed us to segment the imaging domain into three types of tissue volumes: Bones, approximated soft tissues surrounding the joint cavity, and phantom fluid media. The known anatomy from CR made it possible to automatically localize the finite element nodes within each tissue. The initial optical properties used were optimized based on CR-guided forward fitting algorithm for the approximated soft tissues and bone tissues. The entire image reconstruction took about 4 h with 20 iterations on a 2 GHz Pentium 4 PC for each case. Because joint space width is an important measure of the degree of OA, a full width at half maximum method was used to calculate the width of joint space.[23] In evaluating the joint space width, the distance between two adjacent sagittal or coronal slices was different for each subject and was generally less than 1 mm (between 0.5 and 1 mm), depending on the sizes of the joint geometry.[23] The joint spacing estimated from the optical images is given for each of the subjects. The recovered optical absorption and scattering coefficient values are also provided for each tissue of the finger joint, which are calculated based on the mean values for each segmented 3D region. In particular, a schematic demonstration for the sagittal and coronal planes of a 3D DIP finger joint is given in Figs. 1(c) and 1(d).

II.D. Statistical analysis

A receiver operating characteristic (ROC) curve was performed for different parameters from the recovered optical findings. The ROC curves plot the true-positive rate (sensitivity) against the false-positive rate (1−specificity) for different possible cutoff points of a diagnostic test. The accuracy of the test depends on how well the test separates the group being tested into those with and without the disease in question. The areas under the ROC curves (AUCs) demonstrate the test accuracy for different classifiers. In this investigation, imaging features served as the classifiers are extracted from both the recovered optical absorption and scattering images.

For artificial statistical and classification method, sensitivity was directly calculated as TP/(TP+FN), specificity as TN/(TN+FP), positive predictive value as TP/(TP+FP), and negative predictive value as TN/(TN+_FN), where TP represents the number of true-positive findings, TN represents the number of true-negative findings, FP represents the number of false-positive findings, and FN represents the number of false-negative findings.

In addition, several paired sample student t-tests for each classifier were performed to assess the differences between two group subjects including 18 healthy volunteers and 22 patients. The tests were adjusted using Holm's sequential Bonferroni procedure to control the probability of a type I error.

III. RESULTS

III.A. Reconstructed optical images

From the optical absorption and scattering images shown in Figs. 2 and 3, we note that the bones are clearly delineated for both OA and normal joints. While there is no clear boundary between the cartilage and fluid, the joint soft tissues are clearly identified. Figure 2 shows the recovered optical images for a typical OA joint. It is observed that the joint space is narrowed for the OA joints relative to healthy ones (Fig. 3). We found from the majority of our reconstructed results that bone deformation and joint space narrowing are typical radiographic features for OA patients. However, sometimes the joint space narrowing is not so significant compared to that from healthy ones.

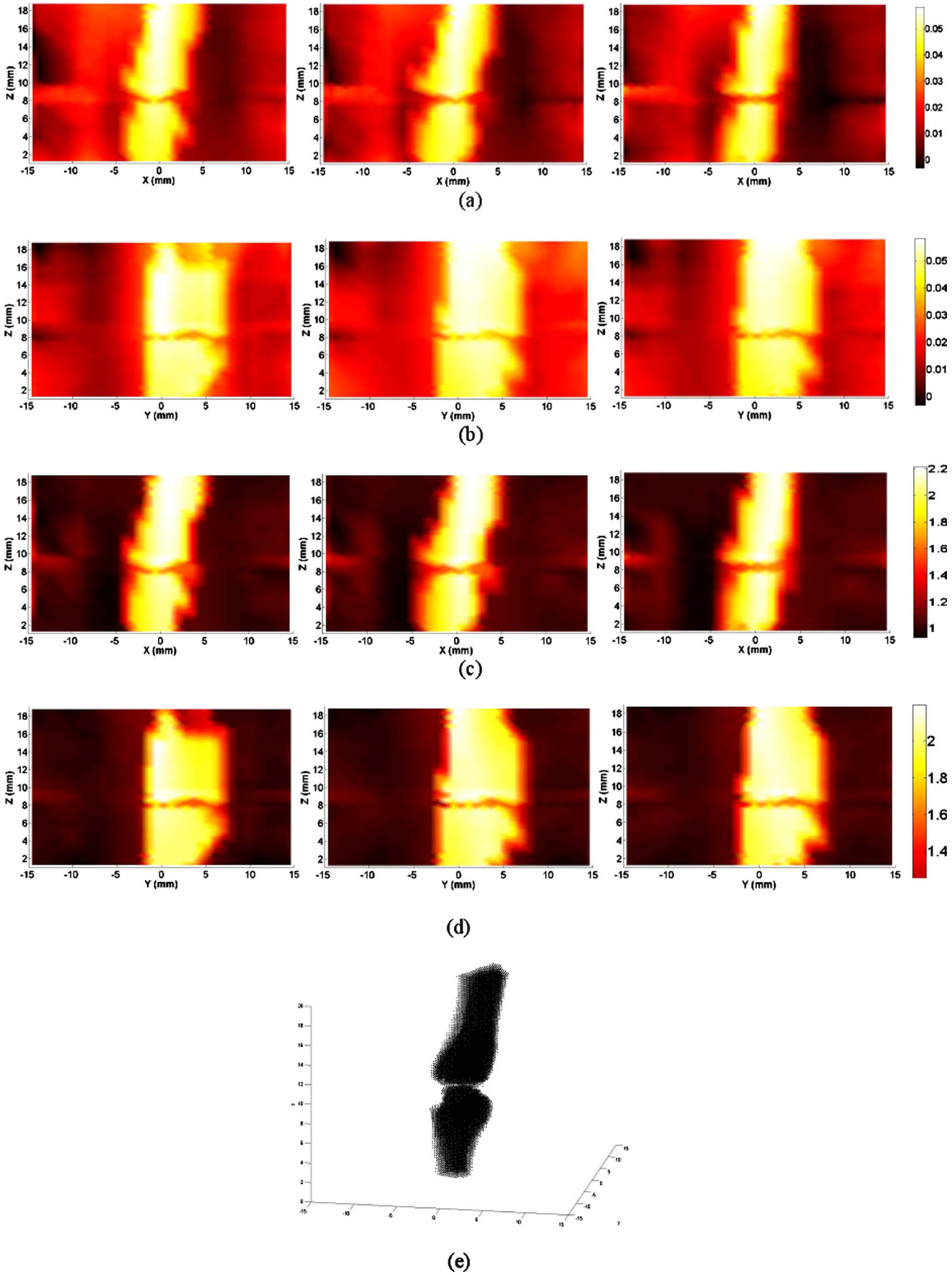

FIG. 2. Reconstructed images at selected coronal/sagittal sections for a typical OA finger joint: (a) Absorption slices along coronal sections; (b) absorption slices along sagittal sections; (c) scattering slices along coronal sections; (d) scattering slices along sagittal sections; and (e) tomographic x-ray image. The axes (left and bottom) indicate the spatial scale in millimeters, whereas the color scale gives the absorption or scattering coefficient in inverse millimeters.

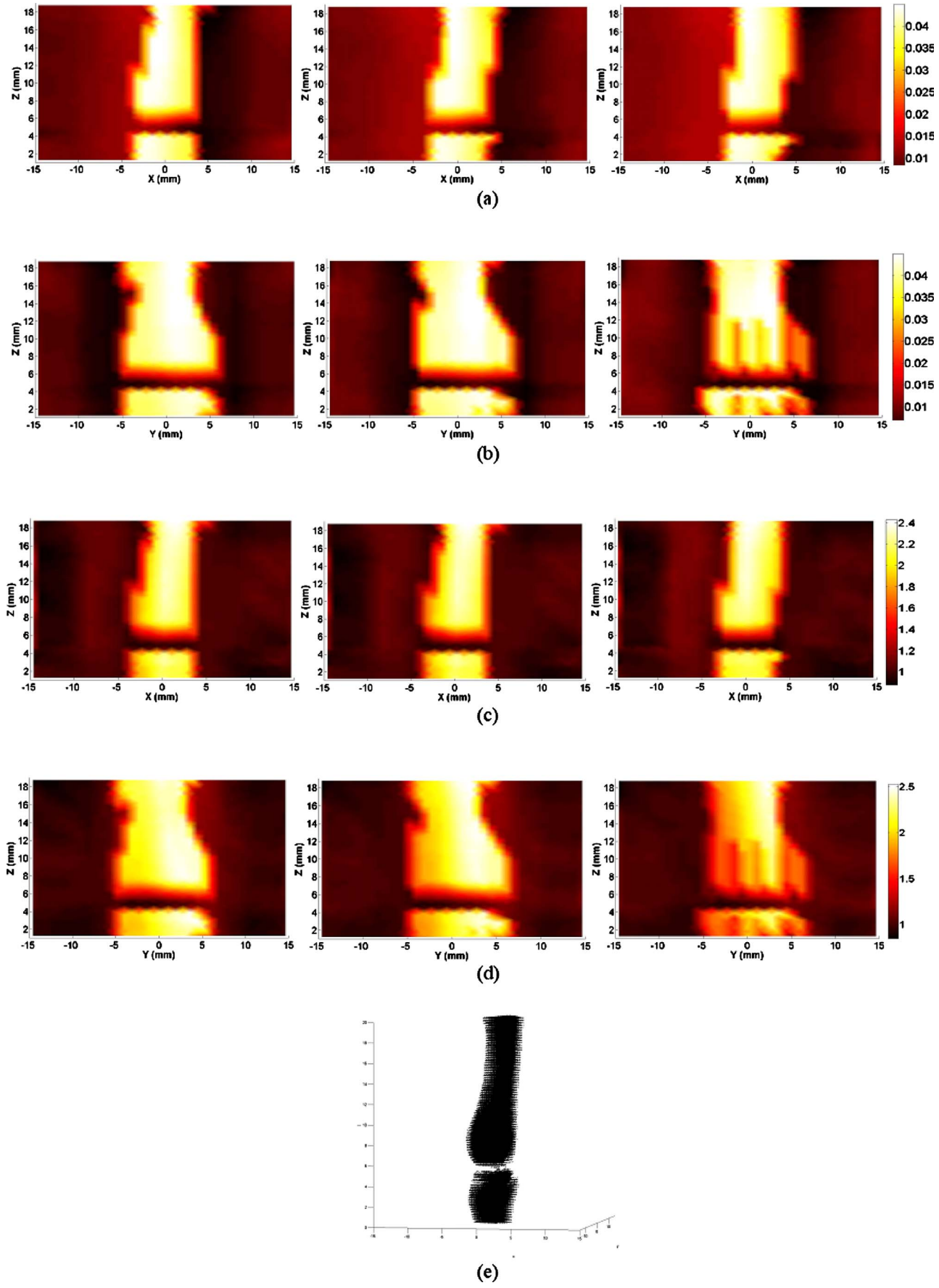

FIG. 3. Reconstructed images at selected coronal/sagittal sections for a typical healthy finger joint: (a) Absorption slices along coronal sections; (b) absorption slices along sagittal sections; (c) scattering slices along coronal sections; (d) scattering slices along sagittal sections; and (e) tomographic x-ray image.

By examining the optical properties of the bones and joint soft tissues, we observe a significant drop in the mean magnitude of absorption and scattering property values of the healthy joint soft tissues, as displayed in Fig. 3; on the contrary, we see only a small drop for the soft tissues surrounding the OA joint cavity in Fig. 2. Interestingly, the difference in scattering and absorption coefficients of the joint tissues between the OA and healthy controls seems more striking from the ratio of scattering or absorption property to that of the bones. These observations also agree well with our statistical findings shown in Figs. 4(a)–4(e), where we find the ratios from the diseased joints are significantly larger than that for normal joints.

III.B. Feature selection

Inspecting Figs. 2–4, we observe significant differences in the detection of pathologic changes between OA and healthy joints based on the optical findings. We find both the reconstructed optical absorption and scattering related parameters are able to distinguish well between OA and normal DIP finger joints in the majority of the subjects. As such, the quantitative parameters including the ratio of mean optical absorption and scattering coefficients between the joint soft tissues and the bones are used as classifiers, since we observe from Fig. 4 that these two parameters show greater differences between OA and healthy joints. In particular, a combined image feature parameter (the product of absorption ratio and scattering ratio) is also used as classifier, which seems to be able to achieve the best separation between healthy and OA joints. In addition, mean joint space width is also used as a classifier to differentiate between OA and healthy joints although the sensitivity based on this feature is very low.

According to the statistical analysis, we can further evaluate whether the aforementioned features are appropriate to serve as distinguishers between OA patients and healthy volunteers. As such, the *t*-tests are completed for all these classifiers and the statistical results are provided in Table I. We found from Table I the absorption ratio and absorption coefficient, scattering ratio and scattering coefficient, combined image feature, and the structural sizes are significant classifiers that can effectively separate the OA group from the healthy group.

III.C. Sensitivity and specificity

We can see from the ROC curves in Fig. 4(e) that the optical parameters can effectively differentiate between healthy and diseased joints, where a sensitivity of 0.75 and a specificity of 1.0 can be reached simultaneously for the optical scattering related parameter, while a sensitivity of 0.68 and a specificity of 1.0 can be reached for the ratio of the optical absorption coefficient. It is also observed from the ROC curves that a sensitivity of 0.45 and a specificity of 1.0 are reached for the joint space width. The best sensitivity-specificity pair is reached when the combined image feature parameter is used, where we can see a sensitivity of 0.92 and a specificity of 1.0 can be obtained. In all these cases, the AUCs are 0.98, 0.93, 0.91, and 0.79 for the combined image feature, optical scattering ratio, optical absorption ratio, and structural size classifier, respectively. In this study, our imaging results are independently provided to the hospital and compared to the diagnosis results from the rheumatologist, which should give a reasonable evaluation of our imaging modality.

IV. DISCUSSION

The current diagnosis of OA is primarily based on clinical examinations and the absence of abnormal laboratory tests, making it difficult to differentiate between OA and healthy joints. Initial attempts to classify OA from healthy subjects using imaging techniques have produced interesting insights, although the diagnostic and prognostic values of classifying patients by imaging findings are incompletely determined. Actually, there is currently no single accepted quantitative classification system for diagnosis of OA by imaging techniques. In addition, for widely used CR techniques, its findings may appear normal for patients with OA and healthy volunteers due to its low sensitivity and specificity. However, our CR-guided DOT imaging method is able to bring quantitatively meaningful measures of both bone and joint tissues. Our results showed statistically significant difference in optical findings between OA and healthy finger joints.

IV.A. Sensitivity and specificity for CR-guided DOT

The statistical analysis results shown in Figs. 4(a)–4(d) and Table I revealed that three mean differences between OA and healthy joints are very significant, including the ratio of optical absorption and scattering coefficient and the combined imaging feature. Better separation is reached when quantitative optical parameters are used as classifiers. In particular, we noted from Fig. 4(e) that sensitivity and specificity values up to 0.92 and 1.0, respectively, can be achieved when the combined image feature parameter is used as a classifier. These observations also agree well with the statistical analysis results in Table I. The high sensitivity and specificity make CR-guided DOT imaging a potentially competitive diagnostic tool for the detection of OA in finger joints.

Compared to the statistical analysis results from DOT only reconstruction,[25] a significant improvement in sensitivity and specificity is observed for the hybrid scanning modality when the combined image feature parameter that incorporates the effect of multiparameters is utilized as the classifier. Conversely, if the comparison is made based on a single parameter, the improvement on sensitivity and specificity is not significant for the optical absorption parameter.[25] However, there is still obvious enhancement in sensitivity when the optical scattering parameter or joint space width captured from the hybrid scanning is used as the classifier.

In addition, the ROC curves conducted here are not based on the statistical results for OA in different stages because the rheumatologist has confirmed that there is no early stage OA subject due to the difficulty in recruiting patients. As such, the cutoff values for sensitivity and specificity analysis

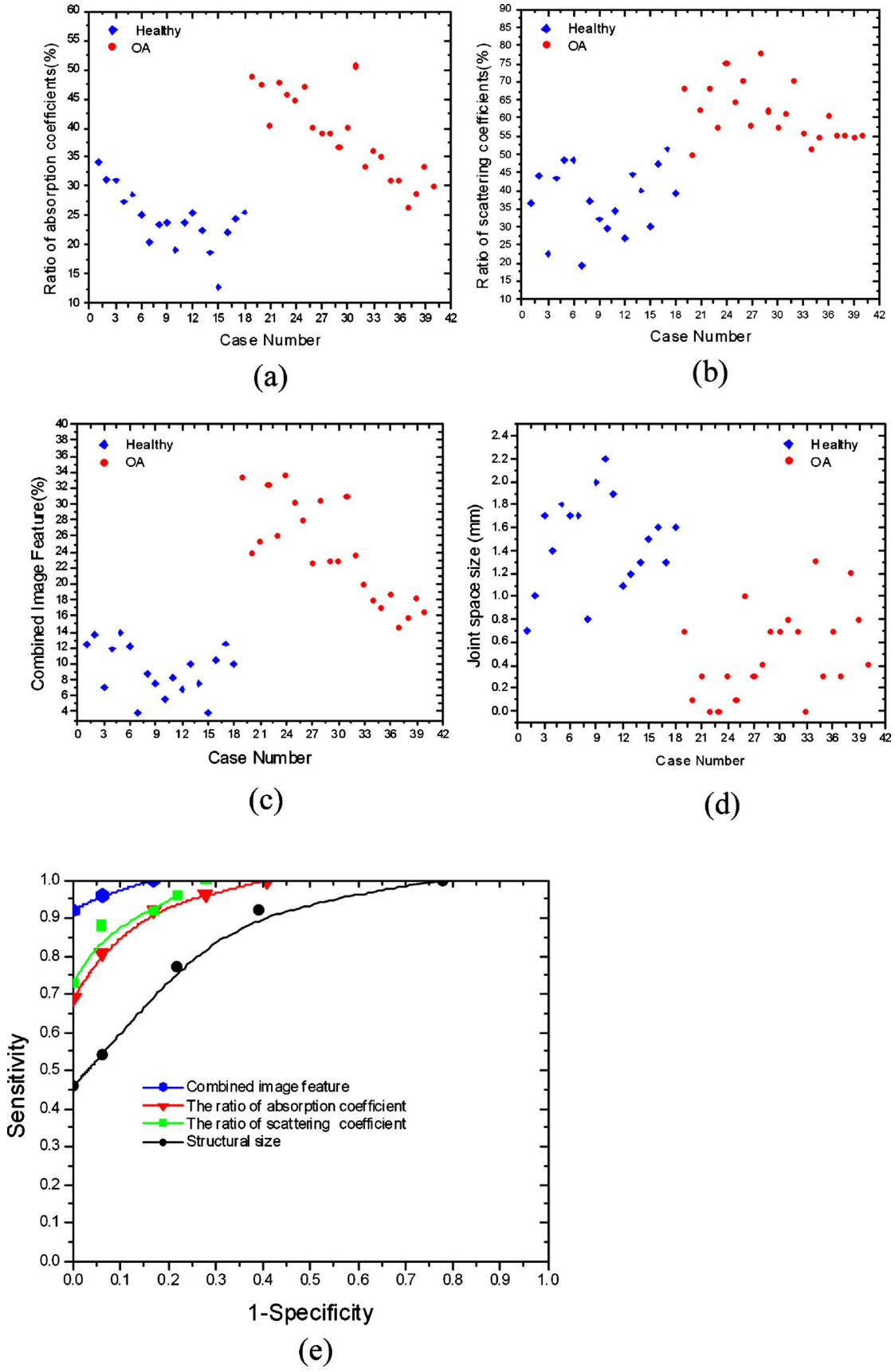

FIG. 4. Plot of the (a) absorption ratio, (b) scattering ratio, (c) combined image feature, and (d) mean joint space width over patient case number. Absorption ratio=absorption coefficient of the joint tissues divided by that of the bone; scattering ratio=scattering coefficient of the joint tissues divided by that of the bone; combined image feature=absorption ratio×scattering ratio. (e) is the ROC curve for the four different classifiers. Structural size=mean joint space width.

TABLE I. Statistical analysis showing the differences between OA and healthy subjects.

Classifiers	Tissues	Cases	*Mean*	*SD*	*p*	*t*
Mean width	Joint	OA	0.5 (mm)	0.38	3.8530×10^{-9}	7.5997
		Healthy	1.5 (mm)	0.42		
Absorption coefficient	Joint	OA	0.0169 (mm^{-1})	0.0043	6.1082×10^{-7}	5.9208
		Healthy	0.0104 (mm^{-1})	0.0021		
	Bones	OA	0.0426 (mm^{-1})	0.0044	0.4816	0.7104
		Healthy	0.0435 (mm^{-1})	0.0032		
Absorption ratio		OA	0.3765	0.0825	9.0024×10^{-9}	7.3239
		Healthy	0.2488	0.0704		
Scattering coefficient	Joint	OA	1.2904 (mm^{-1})	0.1753	1.4725×10^{-9}	7.8014
		Healthy	0.8628 (mm^{-1})	0.1764		
	Bones	OA	2.0950 (mm^{-1})	0.1804	0.4604	0.8163
		Healthy	2.1228 (mm^{-1})	0.4304		
Scattering ratio		OA	0.6098	0.0758	3.7874×10^{-11}	9.1509
		Healthy	0.3702	0.0898		
Combined ratio		OA	0.2380	0.0610	3.5212×10^{-11}	9.2012
		Healthy	0.0923	0.0031		

in this investigation only make sense from mathematical perspective. A further clinical investigation should be conducted to differentiate OA at different stages.

IV.B. Comparable analysis between CR imaging and CR-guided DOT

As displayed in Figs. 2(a)–2(d) and 3(a)–3(d), the CR-guided optical reconstruction results show that the quantitative optical properties between OA and healthy joints are clearly different. As such, CR-guided DOT imaging is a powerful quantitative diagnostic method that may reveal changes in patients with OA who have normal findings from CR evaluation. However, in the area of joint imaging, CR is not able to detect the cartilage and fluids as well as other soft tissue changes surrounding joint cavity, although the changes associated with the soft tissues can be easily captured by CR-guided DOT. CR can only offer qualitative structural information of joints with low contrast in soft tissues [see the images in Figs. 2(e) and 3(e)].

It is also noted from Figs. 1–3 that the joint space width captured by the CR-guided DOT reconstruction is consistent with the CR findings. Our previous investigation showed that the error of the recovered joint space width is less than 10% compared to the CR findings.[23] As such, when the joint space width is utilized as a classifier, the same sensitivity and specificity should be reached for CR and CR-guided DOT imaging. Consequently, based on the recovered structural size, it is possible to distinguish between the diseased and normal control groups, although the sensitivity and specificity are lower compared to those from the quantitative DOT findings, as demonstrated in Fig. 4(e). The individual comparator analysis between CR and CR-guided DOT imaging has been discussed in detail in our previous case study.[23]

Besides the joint space narrowing, osteophyte and cyst formulation are other typical features of CR, which may help improve the sensitivity for OA diagnosis. Though this feature can be identified by an experienced rheumatologist, it cannot be effectively determined by our observations and is not taken as a classifier here. However, this feature can be incorporated into our optical reconstruction process via the *a priori* spatial information and its optical properties can be captured if it exists.

IV.C. Comparable analysis between DOT and CR-guided DOT

In this section, we provided in Fig. 5 the recovered absorption and scattering images without and with CR guidance for another typical healthy subject. Overestimated thickness of the joint tissues and increased boundary artifacts for the optical images without CR guidance are observed. However, CR-guided DOT provides the improved imaging resolution and reconstruction accuracy. First, the high-resolution optical images show accurate delineation of the joint space and bone geometry, where the mean joint space width is about 1.5 mm, consistent with the x-ray finding. In addition, the differences in the optical scattering ratio and absorption ratio between the OA and normal joints estimated from the CR-guided DOT reconstruction are notably increased relative to those without spatial guidance.[25]

IV.D. DOT of finger joints guided by imperfect CR spatial information

In CR-aided DOT, the reconstruction quality of optical images depends on the accuracy of *a priori* spatial information from CR. The position shift of CR image relative to the true joint geometry was possible though the whole shift size is less than 1.5 mm in a single direction for the small volume tissues. The imperfect spatial information generated mainly comes from two perspectives: The hardware error (setups and operation) and the software error (CR image reconstruction). Figures 6(a) and 6(b) present the reconstructed absorption and scattering images at a selected longitudinal plane

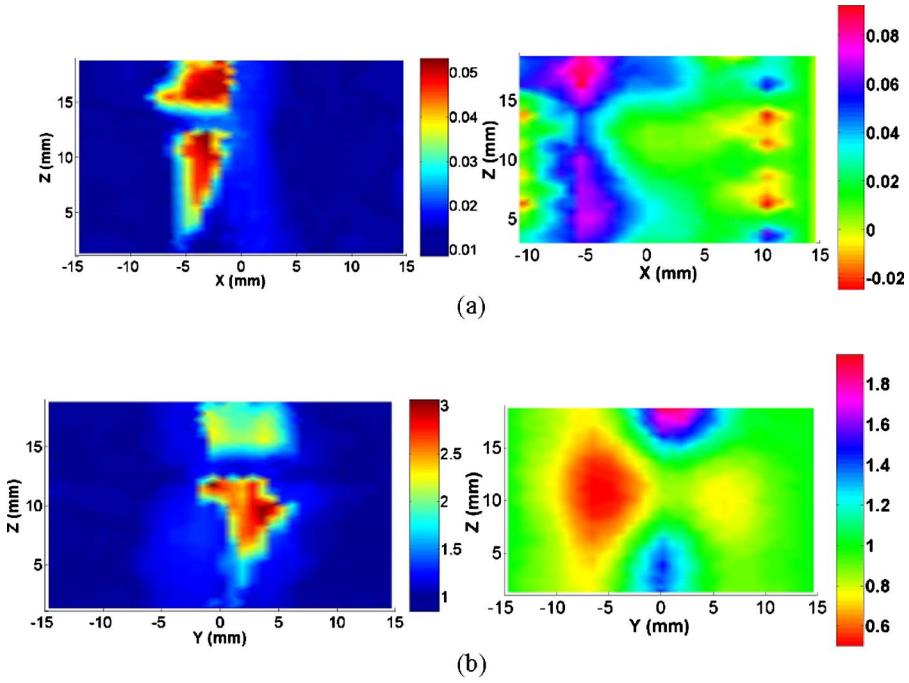

FIG. 5. (a) Reconstructed absorption image at a selected coronal section and (b) scattering image at a selected sagittal section for a healthy joint with (left column) and without (right column) x-ray guidance.

y=0 mm using the perfect (left column) and the imperfect spatial information with a 1.5 mm shift in x-coordinate direction (right column). For this simulation test, a 30 mm (diameter)×20 mm (height) cylinder was used as the background medium. Two centered 10 mm diameter cylindrical objects, embedded in the background medium, were used to mimic bones. The spacing between the two "bones" was 3.0 mm, which was used to simulate cartilage. The optical properties for the background and bones were, respectively, $\mu_a=0.01$ mm^{-1} and $\mu_s'=1.0$ mm^{-1}, and $\mu_a=0.08$ mm^{-1} and $\mu_s'=2.0$ mm^{-1}, while the optical properties for the "cartilage" were $\mu_a=0.003$ mm^{-1} and $\mu_s'=0.8$ mm^{-1}. Our test results indicated that the imperfect spatial information brings small effect on the reconstruction accuracy of joint and bone tissues (total error is less than 10% for the recovered optical properties) while they do produce moderate influence on background fluid media (total error is less than 30% in the recovered optical properties).

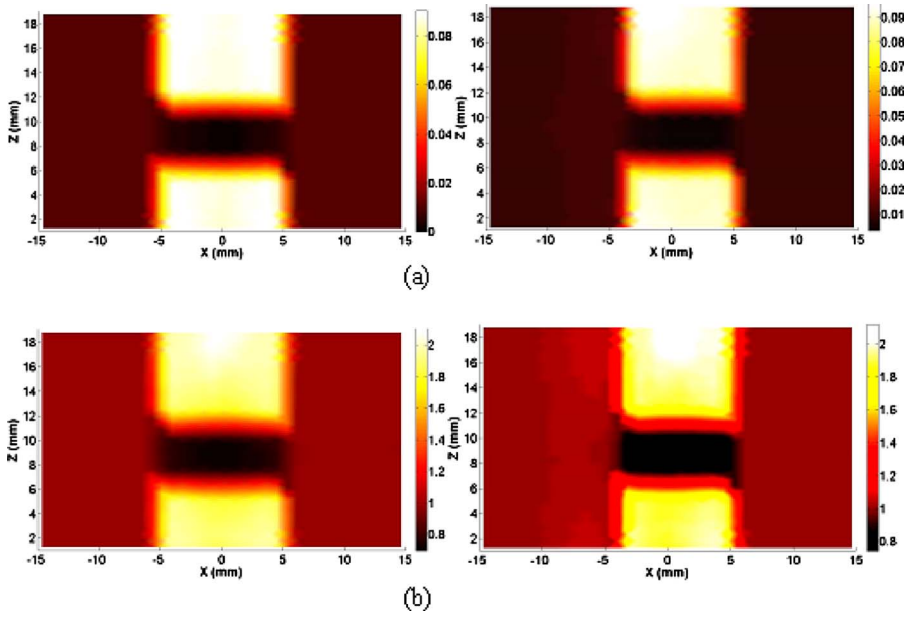

FIG. 6. (a) Reconstructed absorption and (b) scattering image at a selected longitudinal plane for a simulation test with perfect (left column) and imperfect (right column) spatial information.

IV.E. Interpretation of the optical properties changes in OA

The physical process involved in the quantitative changes of optical properties in diseased finger joints may basically come from two kinds of mechanisms. One is from the change of vascular supply of finger joints. The other is based on the optical property changes of soft tissues including the synovial fluid. The bony structural changes in OA will make blood to easily penetrate the subchondral bone plate and the calcified cartilage that lies between subchondral bone and cartilage.[1–3] These vascular supply and bone changes may result in an increased optical absorption in the soft tissues. Moreover, it is well known that with the mild inflammatory changes associated with the onset of OA, the synovial membrane/fluid in articular cavity becomes increasingly turbid.[26] The increased turbidity would accompany increased scattering and absorption coefficients in the diseased synovial membrane/fluid. Interestingly, for a healthy joint, we observed a strong drop in scattering and absorption in the central region of the joint cavity.

IV.F. Conclusions and future directions

In the past several years, we focused on the OA detection and to date have scanned 45 subjects in the States.[21,23] We compared the recovered optical images from the stand alone DOT and CR-guided DOT.[23,25] We also compared the reconstruction results using the different forward models including the transport equation and diffuse approximation.[27,28] In particular, we captured both the structural and functional information of OA patients and healthy controls. It seems that both other groups and ours have obtained similar distribution of optical properties for the healthy subjects. However, it seems that the imaging resolution from other groups was low and they did not capture any meaningful structural information based on their optical finding.[22,29]

In conclusion, the optical findings showed that the optical properties between OA and healthy joints are clearly different, suggesting that these optical parameters could be used to diagnose OA and monitor its progression. Further, larger scale clinical studies are necessary to prove whether the findings identified from the present study can help differentiate OA from healthy joints at an early stage. In addition, it is also necessary to investigate whether the features captured by the present study can help differentiate OA from healthy joints at the large weight-bearing joints of the lower extremities. Finally, it is definitely necessary to validate if this technique can distinguish well between OA, rheumatoid arthritis, and psoriatic arthritis in the joints.

ACKNOWLEDGMENTS

This research was supported in part by the National Institutes of Health (Grant No. R01 AR048122).

[a]Electronic mail: yzhen@bme.ufl.edu
[b]Electronic mail: hjiang@bme.ufl.edu

[1]P. Sarzi-Puttini *et al.*, "Osteoarthritis: An overview of the disease and its treatment strategies," Semin Arthritis Rheum. **35**, 1–10 (2005).
[2]S. B. Abramson, M. Attur, and Y. Yazici, "Prospect for disease modification in osteoarthritis," Nat. Clin. Pract. Rheumatol. **2**, 304–312 (2006).
[3]D. J. Hart and T. D. Spector, "Definition and epidemiology of osteoarthritis of the hand: A review," Osteoarthritis Cartilage **8**, S2–S7 (2000).
[4]A. J. Grainger *et al.*, "MR imaging of erosive in interphalangeal joint osteoarthritis: Is all osteoarthritis erosive," Skeletal Radiol. **36**, 737–745 (2007).
[5]T. Woloszynski, P. Podsiadlo, and G. W. Stachoiak, "A signature dissimilarity measure for trabecular bone texture in knee radiographs," Med. Phys. **37**, 2030–2042 (2010).
[6]R. J. Wakefield *et al.*, "Musculoskeletal ultrasound including definitions for ultrasonographic pathology," J. Rheumatol. **32**, 2485–2487 (2005).
[7]J. A. Tyler, P. J. Watson, H. L. Herrod, M. Robson, and L. D. Hall, "Detection and monitoring of progressive cartilage degeneration of osteoarthritic cartilage by MRI," Acta Orthop. Scand. **266**, 130–138 (1995).
[8]T. Nishii, H. Tanaka, N. Sugano, H. Miki, M. Takao, and H. Yoshikawa, "Disorders of acetabular labrum and articular cartilage in hip hysplasia: Evaluation using isotropic high-resolution CT arthrography with sequential radial reformation," Osteoarthritis Cartilage **15**, 251–257 (2007).
[9]M. Backhaus *et al.*, "Arthritis of the finger joints," Arthritis Rheum. **42**, 1232–1245 (1999).
[10]R. J. Wakefield, P. G. Conaghan, S. Jarrett, and P. Emery, "Noninvasive techniques for assessing skeletal changes in inflammatory arthritis: Imaging techniques," Curr. Opin. Rheumatol. **16**, 435–442 (2004).
[11]G. Karsenty, "An aggrecanase and osteoarthritis," N. Engl. J. Med. **353**, 522–523 (2005).
[12]S. S. Glasson *et al.*, "Deletion of active ADAMTS5 prevents cartilage degradation in a murine model of osteoarthritis," Nature (London) **434**, 644–648 (2005).
[13]B. J. Tromberg, B. W. Pogue, K. D. Paulsen, A. G. Yodh, and D. A. Boas, "Assessing the future of diffuse optical imaging technologies for breast cancer management," Med. Phys. **35**, 2443–2451 (2008).
[14]S. Jiang *et al.*, "Evaluation of breast tumor response to neoadjuvant chemotherapy with tomographic diffuse optical spectroscopy: Case studies of tumor region-of-interest changes," Radiology **252**, 551–560 (2009).
[15]A. Yodh and B. Chance, "Spectroscopy and imaging with diffusing light," Phys. Today **48**, 34–40 (1995).
[16]R. L. Barbour, H. L. Graber, J. Chang, S. S. Barbour, P. C. Koo, and R. Aronson, "MRI-guided optical tomography: Prospects and computation for a new imaging method," IEEE Comput. Sci. Eng. **2**, 63–77 (1995).
[17]D. A. Boas and A. M. Dale, "Simulation study of magnetic resonance imaging-guided cortically-constrained diffuse optical tomography of human brain function," Appl. Opt. **44**, 1957–1968 (2005).
[18]Q. Zhu, N. G. Chen, and S. H. Kurtzman, "Imaging tumor angiogenesis by use of combined near-infrared diffuse light and ultrasound," Opt. Lett. **28**, 337–339 (2003).
[19]Z. Yuan and H. B. Jiang, "Three-dimensional finite element-based photoacoustic tomography: Reconstruction algorithm and simulations," Med. Phys. **34**, 538–546 (2007).
[20]A. Pifferi, A. Torricelli, P. Taroni, A. Bassi, E. Chikoidze, and E. Giambattistelli, "Optical biopsy of bone tissue: A step toward the diagnosis of bone pathologies," J. Biomed. Opt. **9**, 474–480 (2004).
[21]Z. Yuan, Q. Zhang, E. Sobel, and H. B. Jiang, "Three dimensional diffuse optical tomography imaging of osteoarthritis: Initial results in finger joints," J. Biomed. Opt. **12**, 034001-1–034001-10 (2007).
[22]A. K. Scheel *et al.*, "First clinical evaluation of sagittal laser optical tomography for detection of synovitis in arthritic finger joints," Ann. Rheum. Dis. **64**, 239–245 (2005).
[23]Z. Yuan, Q. Zhang, E. Sobel, and H. B. Jiang, "Tomographic x-ray-guided three-dimensional diffuse optical tomography of osteoarthritis in the finger joints," J. Biomed. Opt. **13**, 044006-1–044006-12 (2008).
[24]S. Li and H. Jiang, "A practical method for three-dimensional reconstruction of joints using a C-arm system and shift-and-add algorithm," Med. Phys. **32**, 1491–1499 (2005).
[25]Q. Zhang, Z. Yuan, and H. Jiang, "Three-dimensional diffuse optical tomography of osteoarthritis: A study of 38 finger joints," Proc. SPIE **7166**, 71660K (2009).
[26]A.D. Meisel and P G. Bullough, *Atlas of Osteoarthritis* (Gower Medical, New York, 1984).

[27]Z. Yuan, X. Hu, and H. Jiang, "A higher order diffusion model for three-dimensional photon migration and image reconstruction in optical tomography," Phys. Med. Biol. **54**, 65–88 (2009).
[28]Z. Yuan, Q. Zhang, E. Sobel, and H. Jaign, "Comparison of diffusion approximation and higher order diffusion equation for optical tomography of osteoarthritis," J. Biomed. Opt. **14**, 054013-1–054013-8 (2009).
[29]A. H. Hielscher, A. D. Klose, A. K. Scheel, B. Moa-Anderson, M. Backhaus, U. Netz, and J. Beuthan, "Sagittal laser optical tomography for imaging of rheumatoid finger joints," Phys. Med. Biol. **49**, 1147–1163 (2004).